pubs.acs.org/acschemicalbiology

Article

Systematic Genome Mining of Peptide Metallophore Pathways Uncovers Novel Dibenzo-α-Pyrone Siderophores in *Streptomyces* sp. HB-R818

Dongbo Xu,*[,⊥] Zhenyi Zhou,[⊥] Cai Huang, Peter J. McCarthy, Bin Wei,* and Guojun Wang*

Cite This: https://doi.org/10.1021/acschembio.6c00106

Read Online

ACCESS | Metrics & More | Article Recommendations | Supporting Information

ABSTRACT: Metallophores are metal-chelating natural products that enable microorganisms to acquire essential metal ions and mediate processes such as iron uptake, quorum sensing, and interspecies competition. Metallophores also display potent antimicrobial and anticancer activities, highlighting their biomedical and biotechnological potential. Despite *Streptomyces* being prolific producers of bioactive metabolites, their metallophore pathways remain largely unexplored. Here, we systematically mined 519 reference *Streptomyces* genomes to elucidate the distribution, diversity, and structural features of metallophores and identified a new metallophore biosynthetic gene cluster (BGC) (*ser*) from sponge-derived *Streptomyces* sp. HB-R818. Using a metabolegenomics-based strategy, five new siderophore analogs serobactins A−E (**1**−**5**) and known enterobactin (**6**) were isolated. These compounds show potential to inhibit tumor invasion and feature a unique dibenzo-α-pyrone scaffold in structure, formed through the cyclization of an extra 2,3-dihydroxybenzoic acid with 2,3-dihydroxybenzoyl serine. The BGC (*ser*) was validated by the nonribosomal peptide synthetase gene knockout; the biosynthesis of **1**−**6** was proposed.

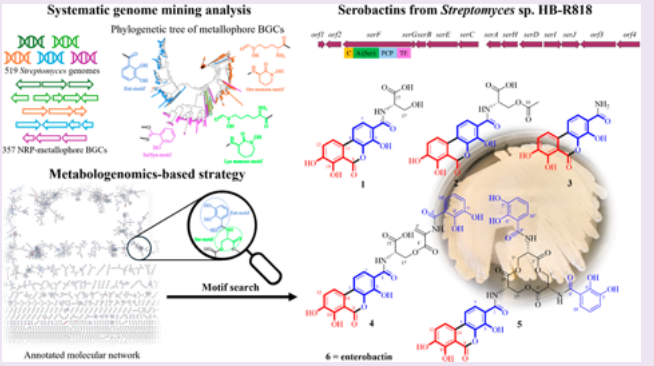

INTRODUCTION

Metallophores are metal-chelating natural products synthesized by microorganisms to facilitate the acquisition of essential metal ions from their surroundings. Among them, Fe(III)-binding siderophores are the most extensively studied, containing key groups such as catechols, hydroxamic acids, and α-hydroxycarboxylic acids for Fe(III) coordination.[1] Beyond iron acquisition, siderophores exhibit antimicrobial applications and therapeutic potentials, such as iron scavenging in rapidly proliferating cancer cells for cancer treatment, antimalarial and antituberculosis activities, and vaccine development.[2] The characteristic $^{54}Fe-^{56}Fe$ isotope pattern associated with Fe(III) ($[M - 2H + Fe]^+$) in mass spectrometry is of great significance for siderophores identification and discovery.[3,4] In contrast, other metallophores remain less explored but play equally important biological roles, such as quorum sensing and antimicrobial defense.[5] Advances in genome-mining approaches have substantially accelerated the discovery of metallophores by enabling the identification of genes involved in their biosynthesis.[6,7] Most metallophores arise from either nonribosomal peptide synthetases (NRPS)-mediated assembly lines, NRP-metallophore biosynthetic gene clusters (BGCs), or an NRPS-independent siderophore-based synthetases route.[8,9]

Marine sponges are a novel and rich source of bioactive molecules with diverse scaffolds; therein-derived natural products exhibit a wide range of therapeutic properties, including antimicrobial, anticancer, anti-inflammatory, etc.[10,11] Sponge-associated bacteria have been considered an important source of bioactive drugs and different enzymes of industrial significance.[12] Among sponge-associated bacteria, the genus *Streptomyces* produces the most antimicrobial compounds.[13] Although the genus *Streptomyces* is widely recognized for its prolific biosynthetic potential, systematic genome mining specifically on metallophore BGCs in *Streptomyces* has not yet been comprehensively investigated.[14,15]

Hence, we assembled a reference *Streptomyces* genome data set and conducted a systematic genome mining analysis to investigate the distribution and diversity of NRP-metallophore BGCs. We summarized the relationships between specific biosynthetic enzymes and the corresponding structural

Received: February 1, 2026
Revised: April 27, 2026
Accepted: May 4, 2026

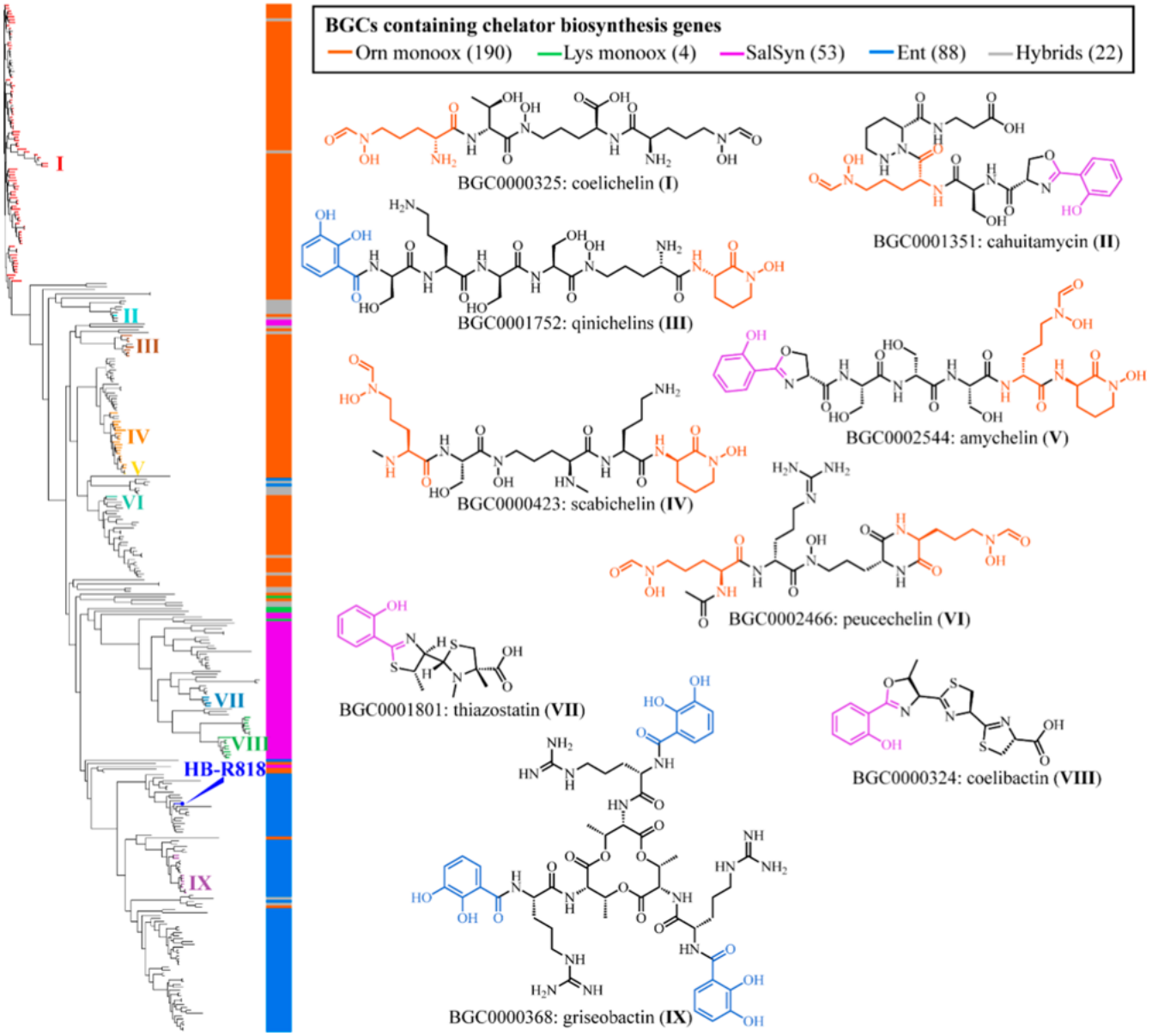

Figure 1. Distribution of *Streptomyces* NRP-metallophore BGCs and 9 gene cluster families (**I**−**IX**) containing MIBiG reference BGCs clustered by BiG-SCAPE, with their corresponding products illustrated. Strain HB-R818 is indicated in the tree.

submotifs. Genome analysis further revealed that HB-R818 harbors a new NRP-metallophore BGC, making it a suitable candidate for exploring its metallophore products. *Streptomyces* sp. HB-R818 was originally selected from the Harbor Branch collection of marine actinomycetes in a search for antimicrobial hits against a panel of pathogens, including *Candida albicans*, *Clostridium difficile*, methicillin-resistant *Staphylococcus aureus* (MRSA), and *Pseudomonas aeruginosa*. The active antifungal ingredient was identified as an antimycin-type compound, urauchimycin D.[16] Next, using a metabologenomics-based strategy, we isolated five novel metallophores and their analogs (**1**−**5**). Notably, compounds **1**−**5** were marked with a dibenzo-α-pyrone scaffold, formed by the cyclization of 2,3-dihydroxybenzoyl serine (2,3-DHB-Ser) and an extra 2,3-dihydroxybenzoic acid (2,3-DHBA). Considering the similarity with reported triscatechol siderophores, the gene cluster (*ser*) of serobactins was located by genome mining, and the biosynthetic pathway was proposed.

RESULTS AND DISCUSSION

Distribution and Features of NRP-Metallophore BGCs in *Streptomyces* Genomes

To explore the potential and features of peptide metallophores in *Streptomyces*, we systematically mined 519 reference genomes using antiSMASH, identifying 357 NRP-metallophore BGCs in 272 genomes (52.4%) (Figure S1). Based on characteristic biosynthetic genes responsible for chelator formation, these BGCs were classified into five types: (i) Ent-type (n = 88), containing EntA (2,3-dihydro-2,3-dihydroxybenzoate dehydrogenase) and entC (isochorismate synthase) for 2,3-DHBA biosynthesis; (ii) Orn_monoox-type (n = 190), encoding ornithine *N*-monooxygenases; (iii) Lys_monoox-type (n = 4), encoding lysine *N*-monooxygenases for hydroxamate formation; (iv) SalSyn-type clusters (n = 53), encoding bifunctional salicylate synthases for salicylate biosynthesis; and (v) hybrid type (n = 22) containing combinations

https://doi.org/10.1021/acschembio.6c00106
ACS Chem. Biol. XXXX, XXX, XXX−XXX

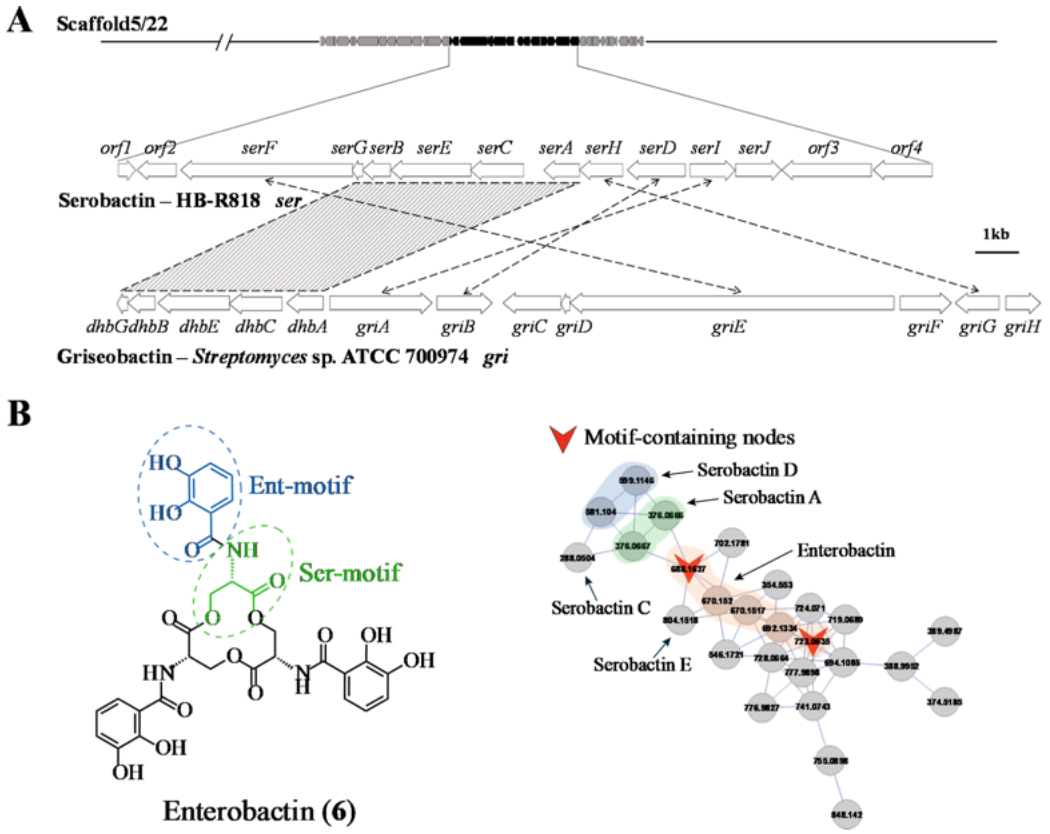

Figure 2. Comparative analysis of the *ser* BGC and metabologenomics-driven identification of candidate metabolites. (A) The illustration of the *ser* and its comparison with the *gri* BGC. (B) A candidate metabolite family whose zoomed-in subnetwork shows similarity to enterobactin (featuring both Ent- and Ser-motifs).

of these biosynthetic features. Among the *Streptomyces* harboring NRP-metallophore BGCs, most typically possess a single cluster, with a subset containing two, and only a few strains carry three or more. *S. inusitatus* JCM 4988 was the only strain in this data set that harbors all four subclasses.

To further investigate the diversity and distribution patterns of NRP-metallophore BGCs, we constructed a phylogenetic tree based on the proto-core peptide sequences of each BGC defined by antiSMASH. Based on the known product annotations from MIBiG entries by BiG-SCAPE clustering, we observed that NRP-metallophore BGCs produce structurally predictable metallophores depending on the core enzymes they encode (Figure 1), which include 9 gene cluster families (**I**-**IX**) that contain MIBiG BGCs. The MIBiG-derived known structures exhibit well-defined metal-chelating moieties that correspond to their BGC types. For example, BGCs belonging to the Orn_monoox-type (families **I**, **IV**, and **VI**) typically produce linear or circular hydroxamate-containing metallophores (orange). SalSyn-type BGCs (families **VII** and **VIII**) generate salicylate-based chelators (purple). Ent-type BGCs (family **IX**) biosynthesize triscatecholate-type metallophores, characterized by 2,3-DHB moieties (blue) tethered to amino acid linkers (like griseobactin). Moreover, hybrid clusters (families **II**, **III**, and **V**) exhibit combinations of these chelating functional groups. Collectively, this pattern indicates that the presence of a specific enzyme strongly correlates with a distinct metallophore scaffold and metal-binding chemistry, offering valuable insights for the next step of metabologenomics-guided discovery.

Targeted Discovery of Peptide Metallophores via a Metabologenomics-Driven Strategy

On the basis of this gene-to-structure logic, we selected an in-house strain, *Streptomyces* sp. HB-R818, which harbors a predicted NRP-metallophore BGC containing *entA* and *entC* genes (Ent-type), suggesting that its products likely contain a 2,3-DHB substructure motif. A total of 33 BGCs (Figure S2) were predicted in the HB-R818 genome by antiSMASH using strict mode (Table S1),[17] including a predicted NRP-metallophore BGC #17 (*ser*) (18.6 kb) (Figure 2A) located in the scaffold 5/22 (453 kb). The *ser* exhibited a high level of similarity with the griseobactin BGC (*gri*), mainly within the proto-core region, as identified by the antiSMASH MIBiG comparison (Table S2).[18] In contrast, at the default BiG-SCAPE distance cutoff of 0.3, the *ser* from strain HB-R818 remained a singleton due to differences in domain-level architecture under stringent similarity criteria (Figure 1), underscoring its novelty in tailoring enzymes and potential for producing novel metabolites. Also, the ClusterBlast result by antiSMASH, compared against the MIBiG database (Figure S3A), showed that only the partial proto-core region shared homology with homologous BGCs in the MIBiG database and reference *Streptomyces* genomes, and its adenylation domain activates serine by domain analysis of the core NRPS SerF. Hence, the *ser* BGC may encode products sharing a conserved core scaffold (likely containing both 2,3-DHB and serine moieties), while peripheral modifications confer substantial structural novelty.

We next performed untargeted metabolomic analysis from the crude extract using liquid chromatography−tandem mass

https://doi.org/10.1021/acschembio.6c00106
ACS Chem. Biol. XXXX, XXX, XXX−XXX

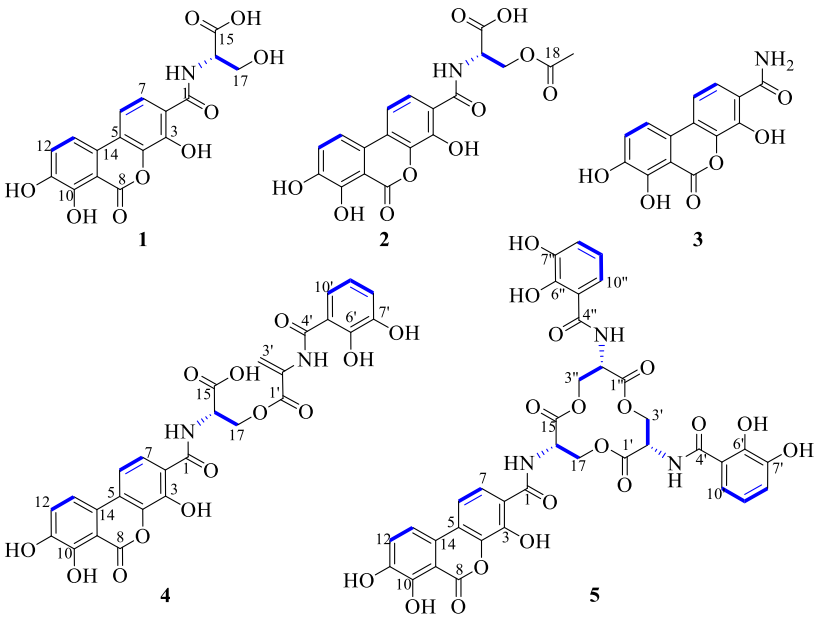

Figure 3. Chemical structures and COSY correlations (blue bold) of **1**−**5**.

Table 1. ^{1}H (600 MHz) and ^{13}C NMR (150 MHz) Spectroscopic Data for Compounds 1−3 in DMSO-d_6

	1			2			3		
position	δ_H (J in Hz)	δ_C, type	HMBC	δ_H (J in Hz)	δ_C, type	HMBC	δ_H (J in Hz)	δ_C, type	HMBC
1		168.2, C			168.4, C			172.1, C	
2		114.6, C			114.2, C			113.2, C	
3		148.8, C			148.8, C			150.6, C	
4		138.2, C			138.2, C			138.0, C	
5		122.7, C			122.9, C			122.9, C	
6	7.73, d (9.0)	111.8, CH	2, 3, 4, 14	7.75, d (9.6)	112.0, CH	1, 2, 3, 4, 14	7.66, d (9.0)	111.4, CH	2, 3, 4, 14
7	7.96, d (8.4)	123.5[a], CH	1, 3, 4, 5	7.90, d (9.0)	123.4, CH	1, 3, 4, 5	7.82, d (8.4)	123.1, CH	1, 3, 4, 5
8		164.5, C			164.5, C			164.6, C	
9		106.8, C			106.8, C			106.8, C	
10		149.3, C			149.4, C			149.3, C	
11		146.6, C			146.7, C			146.5, C	
12	7.40, d (8.4)	123.6[a], CH	10, 11,14	7.40, d (9.6)	123.6, CH	9,10, 11, 14	7.38, d (9.0)	123.6, CH	9, 10, 11, 14
13	7.80, d (9.0)	114.6, CH	5, 8, 9, 11	7.80, d (8.4)	114.6, CH	5, 8, 9, 11	7.80, d (7.8)	114.6, CH	5, 6, 8, 9, 11
14		124.5, C			124.4, C			124.6, C	
15		171.3, C			170.2, C				
16	4.55, dd (11.4, 6)	55.4, CH	15, 17	4.81, m	51.7, CH	15, 17			
17	3.85, m	60.8, CH2	15, 16	4.52, dd (12.6, 4.2)	62.6, CH2	15, 16			
				4.36, dd (10.8, 7.8)		15, 16			
18					170.2, C				
1-NH/NH_2	9.08, d (7.8)		1, 16, 17	9.31, d (8.4)		1,16, 17	8.61, s		1
							8.16, s		2
3-OH				13.27, s					
10-OH	11.11, s			11.10, s		9,10, 11	11.11, s		9, 11
11-OH	10.13, s			10.15, s			10.13, s		10, 11, 12
15-COOH				12.93, s					
18-CH_3				2.01, s	20.6, CH3	17, 18			

[a]Chemical shifts cannot be assigned.

spectrometry (LC−MS/MS). Mass spectral features were extracted using MZmine 4. To maximize structural annotation coverage, we employed the FBMN (v28.2) and MSanalyst platforms[19] using a relatively low similarity threshold to construct a molecular network and perform structure annotation. In total, 1394 features were annotated with putative structures based on the Global Natural Product Social Molecular Networking library (Figure S3B). A custom substructure-matching script was then used to filter metabolites containing the predicted metallophore-related motif (2,3-DHB) and serine-derived substructure (Figure 2B). Ultimately, 16 candidate structures corresponding to 21 nodes across 15 molecular families were identified as containing the 2,3-DHB motif, with only one matching a known compound, enter-

https://doi.org/10.1021/acschembio.6c00106
ACS Chem. Biol. XXXX, XXX, XXX−XXX

Table 2. ^{1}H (600 MHz) and ^{13}C NMR (150 MHz) Spectroscopic Data for 4−5 in DMSO-d_6

	4			5		
position	δ_H (J in Hz)	δ_C, type	HMBC	δ_H (J in Hz)	δ_C, type	HMBC
1		164.9, C			168.7, C	
2		115.1, C			114.0, C	
3		149.1, C			148.9, C	
4		138.3, C			138.2, C	
5		123.2, C			123.2, C	
6	7.76, d (8.4)	111.4[a], CH	**	7.75, d (9.0)	112.2, CH	1, 2, 4
7	7.90, d (9.0)	125.6, CH	1,3,5	7.88, d (9.6)	123.4, CH	1, 3, 5
8		164.8, C			164.5, C	
9		107.2, C			107.0, C	
10		149.8, C			149.8, C	
11		146.6, C			146.8, C	
12	7.42, d (7.2)	124.2, CH	10, 11, 14	7.41, d (8.4)	123.7, CH	10, 11, 14
13	7.79, d (7.8)	115.1, CH	5, 8, 9, 11	7.81, d (9.0)	114.8, CH	9, 11, 12
14		124.3, C			124.5, C	
15		170.8, C			169.6, C	
16	4.92, dd (10.8, 6.6)	52.0, CH	15, 17	4.91, m	51.5[a], CH	15, 17
17	4.69, dd (10.8, 3.0)	64.9, CH_2	15, 16, 1′	4.66, m	63.5[a], CH_2	15, 16
	4.61, dd (10.8, 7.2)			4.40, m		
1′		163.6, C			169.6, C	
2′		132.8, C		4.91, m	51.3[a], CH	1′, 3′
3′	6.48, s	111.5[a], CH_2	1′, 2′	4.66, m	63.3[a], CH_2	1′, 2′
	5.88, s			4.40, m		
4′		169.4, C			169.0, C	
5′		116.0, C			115.4, C	
6′		149.7, C			146.2, C	
7′		147.1, C			148.6, C	
8′	6.93, d (7.8)	119.5, CH	5′, 6′, 7′, 9′	6.96, dd (7.8, 1.2)	119.3, CH	6′, 7′. 9′
9′	6.71, t (7.8)	118.8, CH	5′, 7′	6.74, t (8.4)	118.5, CH	5′, 6′, 7′, 8′
10′	7.37, d (7.2)	118.8, CH	6′, 8′	7.33, dd (8.4, 1.2)	118.4, CH	4′, 6′, 7′, 8′
1-NH	9.18, d (5.4)			9.42, s		1
3-OH	12.33, s					
10-OH	11.09, s		9, 10, 11	11.09, s		9, 10, 11
11-OH	10.19, s		10	10.17, s		
4′-NH	9.38, s		6′, 10′	9.12, d (6.0)		2′, 3′, 4′
6′−OH	11.79, s			11.59, s		5′, 6′, 7′
7′−OH	10.81, s			9.36, s		

[a]Overlapped chemical shifts cannot be assigned; **, δ_H of atoms 6 and 13 are nearly overlapped, which makes it difficult to assign the HMBC signals of atom 6. Atoms 1′−10′ and 1″−10″ from 2-DHB-Ser moieties in compound **5** have nearly identical signals, as do the 4′/4″-NH, 6′/6″−OH, and 7′/7″−OH groups.

obactin (**6**), containing both motifs. Last, focusing on the enterobactin-containing family enabled targeted isolation, leading to the isolation of serobactins A−E (**1**−**5**, Figure 3) and **6** from scaled-up fermentation. This workflow reduced thousands of features to fewer than 100, substantially improving target selection efficiency.

Structural Elucidation from Large-Scale Fermentation

Compound **1** was obtained as a light-yellow powder. Its molecular formula $C_{17}H_{13}O_9N$ was established based on high-resolution electrospray ionization mass spectrometry (HRESI-MS) at m/z 376.0663 $[M + H]^+$ (calcd for $C_{17}H_{14}O_9N$, 376.0669). The nuclear magnetic resonance (NMR) data (Table 1) were similar to those observed in **2** (see below), with key differences in the absence of the singlet methyl group. The formula suggested **1** loses $COCH_2$, indicating a reduction of an acetyl moiety at 17-OH. The remainder of the molecule and all NMR data are consistent with **2**. The HRESI-MS and 1D/2D NMR data of **1** are shown in Figures S4−S9. Hence, **1** was identified as a new siderophore analog, for which the name serobactin A is proposed.

Compound **2** was obtained as a light-yellow powder. Its molecular formula $C_{19}H_{15}O_{10}N$ was determined at m/z 418.0762 $[M + H]^+$ (calcd for $C_{19}H_{16}O_{10}N$, 418.0774). The ^{1}H NMR (Table 1) showed three phenolic hydroxy protons, 3-OH (δ_H 13.27), 10-OH (δ_H 11.10), and 11-OH (δ_H 10.15), and an amide proton 1-CONH (δ_H 9.31). The ^{13}C NMR showed three carbonyl groups, C-1 (δ_C 168.4), C-8 (δ_C 164.5), and C-15 (δ_C 170.2), and four oxygen-bearing aromatic quaternary carbons, C-3 (δ_C 148.8), C-4 (δ_C 138.2), C-10 (δ_C 149.4), and C-12 (δ_C 146.7). The correlations were observed in COSY between 1-CONH (δ_H 9.31), H-16 (δ_H 4.81), and H-17 (δ_H 4.52/4.36). In addition, 1-CONH (δ_H 9.31) was coupled to C-1, C-16 (δ_C 51.7), and C-17 (δ_C 62.6); H-16 was coupled to C-15 and C-17; H-17 was coupled to C-15 and C-16, indicating the presence of a serine group. Moreover, singlet methyl proton CH_3-18 was coupled to C-17 and C-18 (δ_C 170.2), which indicated the connection with one more

https://doi.org/10.1021/acschembio.6c00106
ACS Chem. Biol. XXXX, XXX, XXX−XXX

carbonyl group C-18. These indicated that an acetyl group was condensed and attached to serine−OH. A $^{1}H-^{1}H$ spin correlation was observed between two aromatic methine protons H-6 (δ_H 7.75) and H-7 (δ_H 7.90), indicating the presence of an ortho-disubstituted benzene ring moiety. Additionally, H-6 was coupled to C-2 (δ_C 114.2), C-3, C-4, and C-14 (δ_C 124.4), and H-7 was coupled to C-1, C-3, C-4, and C-5 (δ_C 122.9), indicating the serine group is attached at C-2. Another $^{1}H-^{1}H$ spin correlation was observed between two aromatic methine protons H-12 (δ_H 7.40) and H-13(δ_H 7.80), and H-12 was coupled to C-9 (δ_C 106.8), C-10, C-11, and C-14; H-13 was coupled to C-5, C8, C-9, and C-11. These indicated another ortho-disubstituted benzene ring moiety, and the connectivity between these two benzene rings was supported by heteronuclear multiple bond correlations (HMBCs) between H-13 to C-5 and H-6 to C-14. A carbonyl group C-8 is attached at C-9, which was supported by the HMBC between H-13 and C-8. Finally, a delta-lactone between two benzene rings was identified by unsaturation and exact molecular weight. The HRESI-MS and NMR data of **2** are shown in Figures S10−S15. Hence, **2** was identified as a new siderophore analog, for which the name serobactin B is proposed.

Compound **3** was obtained as a light-yellow powder. Its molecular formula $C_{14}H_9O_6N$ was determined at m/z 288.0506 $[M + H]^+$ (calcd for $C_{14}H_{10}O_6N$, 288.0508). The ultraviolet (UV) spectrum and NMR data (Table 1) showed that **3** has a consistent structure of the dibenzo-α-pyrone moiety from **1**, but loses the chemical shifts of the Ser group. The ^{1}H NMR data showed two amide protons, 1-$CONH_2$ (δ_H 8.61) and (δ_H 8.16). In addition, 1-$CONH_2$ was coupled to C-1 (δ_C 172.1) and C-2 (δ_C 113.2). These indicate that 1-$CONH_2$ is attached at C-2. The remainder of the molecule and all NMR data are consistent with **1**. Positions of phenolic hydroxy protons 10-OH (δ_H 11.11) and 11-OH (δ_H 10.13) were supported by correlations in HMBC between 10-OH and C-9 (δ_C 106.8)/C-11 (δ_C 146.5) and 11-OH and C-10 (δ_C 149.3)/C-11/C-12 (δ_C 123.6). The HRESI-MS and NMR data of **3** are shown in Figures S16−S21. Hence, **3** was identified as a new siderophore analog, for which the name serobactin C is proposed.

Compound **4** was obtained as a light-yellow oil. Its molecular formula $C_{27}H_{20}N_2O_{13}$ was established at m/z 581.1042 $[M + H]^+$ (calcd for $C_{27}H_{21}N_2O_{13}$, 581.1044) and 634.0159 $[M - 2H + Fe]^+$ (calcd for $C_{27}H_{18}N_2O_{13}Fe$, 634.0153). The ^{1}H NMR and the formula suggested that **4** may contain one more 2,3-DHB-Ser unit. The formula and NMR (Table 2) proved that **4** contained the full structure of **1** and one more 2,3-DHB-Ser-like unit. The HMBCs between H-17 and carbonyl group C-1′ supported the connection between the two subunits by an ester bond. The presence of two additional olefinic proton signals (δ_H 6.48 and 5.88), the correlations in HSQC between these two protons and C-3′ (δ_C 111.5), and the HMBCs between two protons and C-1′/C-2′ identified a vinyl group in the Ser side chain. The structure of **4** was confirmed by unsaturation. The HRESI-MS and NMR data of **4** are shown in Figures S22−S27. Hence, **4** was identified as a new siderophore analog, for which the name serobactin D is proposed.

Compound **5** was obtained as a light-yellow powder. Its molecular formula $C_{37}H_{29}N_3O_{18}$ was determined at m/z 804.1523 $[M + H]^+$ (calcd for $C_{37}H_{30}N_3O_{18}$, 804.1524) and 857.0637 $[M - 2H + Fe]^+$ (calcd for $C_{37}H_{27}N_3O_{18}Fe$, 857.0634). The ^{1}H NMR (Table 2 and Figure S29) and the formula suggested the structure of **5** contained two more 2,3-DHB-Ser units compared to **1**. The ^{1}H NMR data showed three amide protons (δ_H 9.11, 9.12, and 9.42), three Ser side chain H signals, and two sets of specific aromatic protons (δ_H 6.74 and 7.33) in 2,3-DHB subunits. Four similar aromatic protons on the benzene ring proved the presence of the dibenzo-α-pyrone substructure in **5**. Combined with the unsaturation, the structure of **5** was confirmed by the intermolecular cyclization of **1** substructure and two more 2,3-DHB-Ser. The HRESI-MS and NMR data of **5** are shown in Figures S28−S34. Hence, **5** was identified as a new siderophore analog, for which the name serobactin E is proposed.

Additionally, enterobactin (**6**) was isolated and NMR data are consistent with the literature.[20,21] The HRESI-MS and NMR data of **6** are shown in Figures S35−S41. The core NRPS SerF domain analysis using the PKS(polyketide synthase)/NRPS Analysis Web Server[22] predicted that the adenylation domain activates serine and forms the 2,3-DHB-Ser by the condensation domain (Figure 4A), compared with

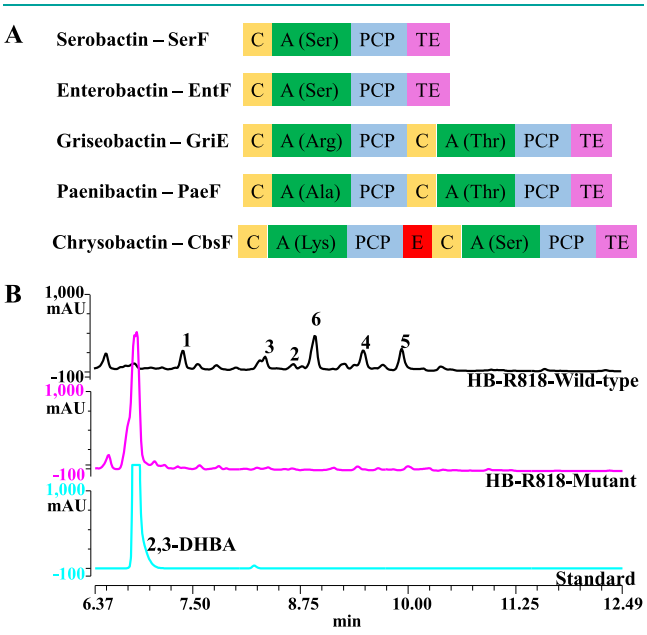

Figure 4. NRPS gene deletion validates the *ser* biosynthesis. (A) The domain architecture of NRPSs in the biosynthesis of triscatechol siderophores. C—condensation; A—adenylation; PCP—peptidyl carrier protein; E—epimerization; TE—thioesterase. (B) HPLC fingerprint profile (254 nm) of secondary metabolites from HB-R818 wild-type and mutant.

the reported NRPSs in the biosynthesis of triscatechol siderophores like griseobactin,[18] enterobactin,[23] paenibactin,[24] and chrysobactin.[25] Although Marfey's analysis has not been performed to confirm the stereochemistry, the absence of the epimerization (*E*) domain in SerF strongly indicates an *L* configuration for the primary serine building block in **1**, **2**, and **4**−**6**, consistent with the reported *L*-configurations of enterobactin and triscatechol siderophores.[1]

Characterization of the *ser* Encoding the Serobactins Biosynthesis

To validate whether this *ser* is responsible for serobactins, an in-frame deletion of the NRPS gene *serF* was performed via

https://doi.org/10.1021/acschembio.6c00106
ACS Chem. Biol. XXXX, XXX, XXX−XXX

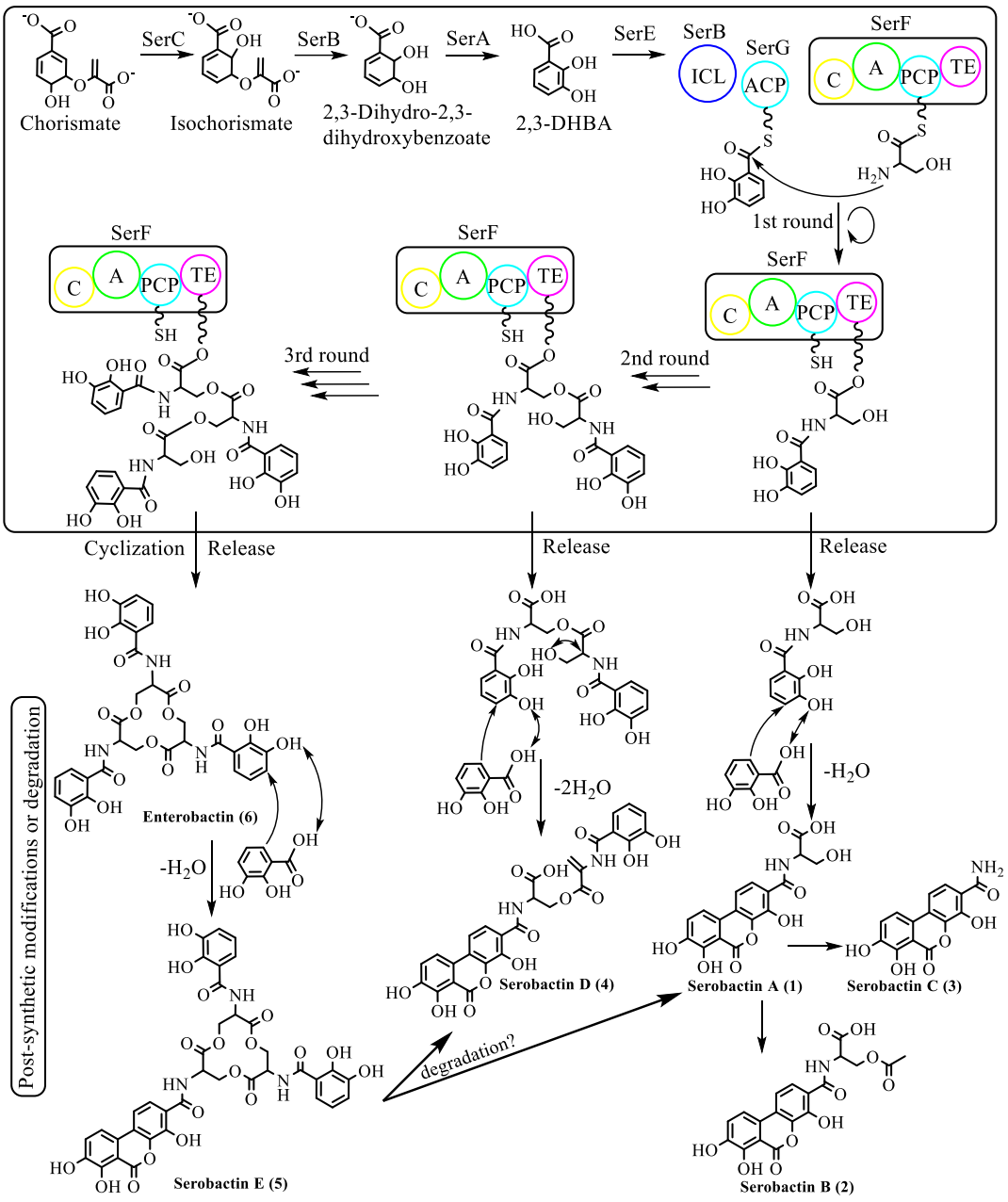

Figure 5. Proposed biosynthetic pathway of serobactins in strain HB-R818, inferred from enterobactin's biosynthetic pathway.

double crossover homologous recombination. Three mutants were obtained and fermented to analyze the secondary metabolites. High-performance liquid chromatography (HPLC) fingerprint profiles indicated that the production of **1**–**6** was abolished in all three mutants, leading to the accumulation of 2,3-DHBA. A representative profile is shown in Figure 4B. This result confirmed that the *ser* is responsible for the biosynthesis of serobactins and that **1**–**6** were biosynthesized through the 2,3-DHB-Ser unit; serobactin B (**2**) or C (**3**) was probably either post-modified or degraded from **A** (**1**). Also, the linear serobactin A (**1**) or D (**4**) was either released as oligomeric forms or cleaved from cyclic serobactin E (**5**) like the degradation in cyclic salmochelin S4 (a C-glucosylated enterobactin).[26,27] According to the biosynthetic pathways of known triscatechol siderophores,[1,18,23] a putative biosynthetic pathway was proposed for **1**–**6** (Figure 5).

Bioactivity Evaluation

The bioactivities were assessed through different bioassays. No obvious antibacterial and antifungal activities were found (minimum inhibitory concentration >50 μg/mL). Interestingly, **1** and **5** significantly promoted talin-β1-integrin interaction in the glutathione S-transferase (GST) pulldown assay (50 μg/mL) and significantly inhibited the Matrigel invasion of 4T1 cells (25 μg/mL, Figure S42). In our GST pulldown assay, cyanidin-3-glucoside was previously reported to promote talin-integrin interaction while inhibiting cell invasion.[32] In addition, high levels of talin2 suppress tumorigenesis in vivo,[35] which suggests that strengthened talin–β1 integrin interaction contributes to reduced invasion. Hence, these findings suggest that these compounds have the potential to inhibit tumor invasion.

In conclusion, we collected a reference *Streptomyces* genome data set and performed a systematic genome mining analysis to

https://doi.org/10.1021/acschembio.6c00106
ACS Chem. Biol. XXXX, XXX, XXX−XXX

explore the distribution and diversity of NRP-metallophore BGCs. Proto-core-based phylogenetic analysis was then applied to reveal the relationship between key biosynthetic enzymes and characteristic structural motifs in metallophore products. We identified and highlighted a new metallophore BGC in the marine sponge-derived *Streptomyces* sp. HB-R818 in phylogenetic analysis. Next, we developed a metabologenomics-guided discovery strategy that integrates BGC-derived substructure information with NRPS substrate specificity to filter and prioritize candidate molecular families from nontargeted metabolomic data sets using LC−MS/MS. Using this strategy, we isolated five new metallophores and their analogs (**1**−**5**) from strain HB-R818. Notably, compounds **1**−**5** were marked with a unique dibenzo-α-pyrone scaffold, formed by the cyclization of 2,3-DHB-Ser and an extra 2,3-DHBA. Bioassay tests indicate these compounds inhibit tumor invasion. Moreover, the biosynthetic role of the *ser* BGC in the genome was confirmed by knocking out the NRPS gene *serF*, and its biosynthetic pathway was also proposed. The identification and characterization of enzymes for post-modifications or degradation in the *ser* BGC are warranted in the future.

EXPERIMENTAL SECTION

Genome Collection and Mining

Streptomyces reference genomes and their metadata were retrieved from GenBank using NCBI Data sets command-line tools (v18.7.0). BGCs were predicted and annotated using antiSMASH (v7.0.1). A genome-based phylogenetic tree was constructed with UBCG1 (v3.0) and annotated with genome and BGCs information to visualize the distribution of NRP-metallophore BGCs in *Streptomyces*. In addition, a BGC-level phylogenetic analysis was performed based on proto-core regions defined by antiSMASH, which encompass the core biosynthetic genes as well as intervening noncore genes within a defined distance threshold. Proto-core regions were extracted from each BGC based on the "proto_core" feature in the antiSMASH output region GenBank (gbk) files, and their protein sequences were concatenated for multiple sequence alignment using MAFFT (v7.505), followed by the phylogenetic tree construction with FastTree (v2.1.11). To compare *Streptomyces* BGCs with the known clusters in the MIBiG database (v4), BiG-SCAPE (v2.0.0b8) was applied using a default distance cutoff of 0.3 to explore the BGC diversity and summarize the relationships between chelator biosynthesis genes and their corresponding chelating motifs.

Genome Sequencing and Analysis

The genome of HB-R818 was sequenced using both Miseq and PacBio platforms and then assembled by RTL Genomics. The genome assembly contained 16 contigs; the total contig length was 8,946,061 bp with a median G + C content of 71%. The HB-R818 genome was analyzed for 33 BGCs by antiSMASH 8 using strict mode.[17]

General Experimental Procedures

HRESI-MS data were recorded on an LTQ Orbitrap VELOS (Thermo Fisher) high-resolution mass spectrometer. NMR spectra were taken on a JEOL ECA-600 spectrometer in DMSO-d_6 (2.50 ppm for ^{1}H, 39.5 ppm for ^{13}C) at 600 MHz for ^{1}H and 150 MHz for ^{13}C. An Isco Combiflash RFx4 with a RediSep Rf Gold C18 column (size 50 g) was applied to fractionate the crude extract. Analytical and semipreparative reversed-phase HPLC were performed on an UltiMate 3000 system (Thermo Fisher) with an Apollo C18 column (250 mm × 4.5 mm) and an Apollo C18 column (250 mm × 10 mm), respectively. Sephadex LH-20 (GE Healthcare) was used for column chromatography.

Microorganisms and Fermentation

The producing *Streptomyces*, designated as HB-R818, was isolated from a marine sponge, *Forcepia* sp., collected from the Gulf of Mexico, Florida, at 232 feet and is held in the Harbor Branch Oceanographic Institute Marine Microbial Culture Collection. The strain was cultivated on Marine Agar 2216 (MA) plates at 28 °C. For a large-scale fermentation, the strain spores were collected from agar plates and suspended in sterile PBS. Then suspension aliquots were inoculated into 180 250 mL flasks containing 100 mL of SPY media supplemented with 2 mM $LaCl_3$ (Recipes reported in literature[30]). All flasks were cultured on a rotatory shaker (200 rpm) for 7 days at 28 °C.

Extraction, Isolation, and Purification

The broth (18 L) was directly extracted with an equal volume of EtOAc with sonication four times. The organic layer was combined and evaporated in vacuo to dryness. Samples were redissolved in methanol for general HPLC fingerprint profile analysis, which was performed in a H_2O + 0.1% trifluoroacetic acid−TFA (solvent A)/MeCN (solvent B) system, which was eluted by a gradient of 5 min equilibration, 5% B; 0 min, 5% B; 15 min, 100% B; 20 min, 100% B with a flow rate of 1.5 mL/min. Crude extracts (12.9 g) were separated into three parts, and all were subjected to Isco Combiflash RFx4 using a H_2O/MeCN system due to the loading limits. Fractions were purified by column chromatography on Sephadex LH20 eluted with MeOH/CH_2Cl_2. Then, the combined tubes were subjected to semipreparative HPLC. Compound **1** (6 mg, t_R = 19.65 min) was purified in a 20 min gradient from 20% to 28% MeCN at a flow rate of 3 mL/min. Compounds **2** (4 mg, t_R = 12.06 min) and **3** (4 mg, t_R = 10.49 min) were obtained separately from each fraction by using the same 12 min gradient from 30% to 45% MeCN at a flow rate of 3 mL/min. Compound **4** (5 mg, t_R = 18.68 min) was purified in a 25 min gradient from 35% to 41% MeCN at a flow rate of 3 mL/min. Compound **5** (1.5 mg, t_R = 26.04 min) was obtained in a 30 min gradient from 35% to 41% MeCN at a flow rate of 3 mL/min. Compound **6** (2.0 mg, t_R = 20.85 min) was obtained in 35% MeCN at a flow rate of 3 mL/min.

Serobactin A (1)

Light-yellow powder; UV (CH_3CN/H_2O) λmax 217.62, 311.28, 356.39 nm; ^{1}H and ^{13}C NMR, HMBC, see Table 1; HR-ESI-MS m/z 376.0663 $[M + H]^+$ (calcd for $C_{17}H_{14}O_9N$, 376.0669).

Serobactin B (2)

Light-yellow powder; UV (CH_3CN/H_2O) λmax 242.04, 309.55, 358.62 nm; ^{1}H and ^{13}C NMR, HMBC, see Table 1; HR-ESI-MS m/z 418.0762 $[M + H]^+$ (calcd for $C_{19}H_{16}O_{10}N$, 418.0774).

Serobactin C (3)

Light-yellow powder; UV (CH_3CN/H_2O) λmax 223.85, 310.34, 355.36 nm; ^{1}H and ^{13}C NMR, HMBC, see Table 1; HR-ESI-MS m/z 288.0506 $[M + H]^+$ (calcd for $C_{14}H_{10}O_6N$, 288.0508).

Serobactin D (4)

Light-yellow oil; UV (CH_3CN/H_2O) λmax 219.34, 315.72, 358.47 nm; ^{1}H and ^{13}C NMR, HMBC, see Table 2; HR-ESI-MS m/z 581.1042 $[M + H]^+$; 634.0159 $[M - 2H + Fe]^+$ (calcd for $C_{27}H_{21}N_2O_{13}$, 581.1044; $C_{27}H_{18}N_2O_{13}Fe$, 634.0153).

Serobactin E (5)

Light-yellow powder; UV (CH_3CN/H_2O) λmax 218.86, 312.83, 355.77 nm; ^{1}H and ^{13}C NMR, HMBC, see Table 2; HR-ESI-MS m/z 804.1523 $[M + H]^+$; 857.0637 $[M - 2H + Fe]^+$ (calcd for $C_{37}H_{30}N_3O_{18}$, 804.1524; $C_{37}H_{27}N_3O_{18}Fe$, 857.0634).

Enterobactin (6)

Light-yellow powder; UV (CH_3CN/H_2O) λmax 204.36, 314.06 nm; ^{1}H and ^{13}C NMR see Figures S37−S41; HR-ESI-MS m/z 607.1520 $[M + H]^+$; 723.0633 $[M - 2H + Fe]^+$ (calcd for $C_{30}H_{28}N_3O_{15}$, 670.1520; $C_{30}H_{25}N_3O_{15}Fe$, 723.0630).

https://doi.org/10.1021/acschembio.6c00106
ACS Chem. Biol. XXXX, XXX, XXX−XXX

Antimicrobial Bioassay

The antimicrobial activity of purified compounds was tested against *C. albicans*, MRSA, and *P. aeruginosa* using a standard disk-diffusion method, following the previous study.[16,31]

Talin-Integrin Interaction Assay and Invasion Assay

The binding of purified His-tagged proteins to GST-β1-integrin tails was performed following the previously established assay.[32] The invasion assay in Matrigel was performed following the previously established assay.[33,34] Talin, a β-intergrin and actin-binding protein, binds to the beta subunit of integrins, a family of transmembrane adhesion receptors that mediate cell−matrix adhesion, thus activating integrins and regulating cell migration, invasion, and growth.[28,29] Cyanidin-3-glucoside was previously reported to promote talin-integrin interaction but inhibited cell invasion, probably through perturbing integrin activation, a key process involved in cell invasion and metastasis.[32] Exogenous expression of high levels of talin2 also inhibited tumorigenesis more efficiently than talin2 KD or KO in the mouse xenograft model, which suggests that promoting instead of inhibiting the talin-integrin interaction could offer a more efficient strategy for cancer therapy.[35] Given that high levels of talin2 suppress tumorigenesis in vivo, these findings indicate that increased talin−β1 integrin interaction suppresses cell invasion.

In-Frame Deletion of the NRPS Gene

The in-frame deletion was performed in strain HB-R818 following the previous protocol.[30,36] Briefly, a 1176 bp left homologous arm was amplified using primers C17F-for/C17F-rev, and a 1266 bp right homologous arm was amplified using primers C17R-for/C17R-rev. After sequencing confirmation of PCR products, the L-arm and R-arm fragments were digested by *Nde*I/*Spe*I and *Spe*I/*Hin*dIII, respectively, and ligated into the pYH7[37] fragment digested by *Nde*I/*Hin*dIII. The recombinant plasmid pYH7-C17 was transformed into *Escherichia coli* ET12567/pUZ8002. Intergeneric conjugation of plasmid pYH7-C17 into strain HB-R818 by *E. coli* ET12657/pUZ8002 was carried out as described in Practical *Streptomyces* Genetics.[38] The donor ET12657/pUZ8002 containing plasmid and the recipient spores were mixed and spread on Mannitol-Soy-agar (MS) plates with 10 mM $MgCl_2$ and grown for 15 h at 28 °C. Then, the plates were overlaid with 1 mL of sterile water containing 50 μg/mL apramycin and 50 μg/mL nalidixic acid. A single clone with the deletion of the NRPS gene was confirmed by PCR using primers C17FR-for and C17FR-rev (Table S3). A knockout mutant was randomly chosen for further fermentation and analytical experiments.

■ ASSOCIATED CONTENT

Data Availability Statement

The data and code related to the genome mining, as well as the Jupyter Notebook used for substructure searching, are available at https://github.com/BioGavin/streptomyces_NRPmetallophore_mining. The draft genome sequence of strain HB-R818 has been submitted to GenBank with an accession number JAOCNE000000000. The biosynthetic gene cluster sequence has been submitted to GenBank with an accession number OP485289.

Supporting Information

The Supporting Information is available free of charge at https://pubs.acs.org/doi/10.1021/acschembio.6c00106.

Predicted BGCs, ORFs in *ser*, primers, NRP-metallophore BGCs, draft genome, *ser* BGC, metabolites via FBMN, HRESI-MS, ^{1}H NMR, ^{13}C NMR, ^{1}H−^{1}H COSY, HSQC, HMBC spectra, and biological activity (PDF)

■ AUTHOR INFORMATION

Corresponding Authors

Dongbo Xu − *Harbor Branch Oceanographic Institute, Florida Atlantic University, Fort Pierce, Florida 34946, United States;* Present Address: Roswell Park Cancer Institute, Elm & Carlton Streets, Buffalo, New York, 14263, United States; orcid.org/0000-0003-4829-7459; Phone: +1-716-341-8169; Email: Dongbo.xu@roswellpark.org

Bin Wei − *College of Pharmaceutical Science & Collaborative Innovation Center of Yangtze River Delta Region Green Pharmaceuticals, Zhejiang University of Technology, Hangzhou 310014, China;* orcid.org/0000-0001-7362-1228; Phone: +86-1996-730-8927; Email: binwei@zjut.edu.cn

Guojun Wang − *Harbor Branch Oceanographic Institute, Florida Atlantic University, Fort Pierce, Florida 34946, United States;* orcid.org/0000-0001-6416-2744; Phone: +1-772-242-2423; Email: wanggj2003@gmail.com

Authors

Zhenyi Zhou − *College of Pharmaceutical Science & Collaborative Innovation Center of Yangtze River Delta Region Green Pharmaceuticals, Zhejiang University of Technology, Hangzhou 310014, China;* orcid.org/0000-0003-1342-6054

Cai Huang − *Markey Cancer Center, University of Kentucky, Lexington, Kentucky 40506, United States*

Peter J. McCarthy − *Harbor Branch Oceanographic Institute, Florida Atlantic University, Fort Pierce, Florida 34946, United States*

Complete contact information is available at: https://pubs.acs.org/10.1021/acschembio.6c00106

Author Contributions

$^{\perp}$D.X. and Z.Z. contributed equally. D.X., B.W., and G.W. conceptualized and designed the study; D.X. conducted compound-related experiments and generated data; Z.Z. conducted systematic bioinformatics analysis and generated data; C.H. performed the cancer cell invasion assay; D.X. and Z.Z. wrote the original draft; D.X., P.J.M., B.W., and G.W. reviewed and edited the manuscript.

Notes

The authors declare no competing financial interest.

■ ACKNOWLEDGMENTS

The authors thank Dr. Amy E. Wright from Harbor Branch Oceanographic Institute for the help with NMR analysis and Dedra Harmody from Harbor Branch Oceanographic Institute for routine antimicrobial testing. This work was supported in part by NIH grant CA209189 and the Start-Up package provided by Florida Atlantic University to G.W. The bioinformatics analysis was supported by the National Key Research and Development Program (No. 2022YFC2804700) to B.W.

■ REFERENCES

(1) Reitz, Z. L.; Sandy, M.; Butler, A. Biosynthetic considerations of triscatechol siderophores framed on serine and threonine macrolactone scaffolds. *Metallomics* **2017**, *9*, 824−839.

(2) Ribeiro, M.; Simões, M. Advances in the antimicrobial and therapeutic potential of siderophores. *Environ. Chem. Lett.* **2019**, *17*, 1485−1494.
(3) Sidebottom, A. M.; Karty, J. A.; Carlson, E. E. Accurate mass MS/MS/MS analysis of siderophores ferrioxamine B and E1 by collision-induced dissociation electrospray mass spectrometry. *J. Am. Soc. Mass Spectrom.* **2015**, *26*, 1899−1902.
(4) Pluhacek, T.; Lemr, K.; Ghosh, D.; Milde, D.; Novak, J.; Havlicek, V. Characterization of microbial siderophores by mass spectrometry. *Mass Spectrom. Rev.* **2016**, *35*, 35−47.
(5) Kamyabi, G.; Debley, E. L.; Nolan, E. M. Recent advances in metallophore research uncover functions in quorum sensing, antimicrobial activity, and lanthanide acquisition. *Curr. Opin. Chem. Biol.* **2025**, *87*, 102604.
(6) Cavas, L.; Kirkiz, I. Characterization of siderophores from *Escherichia coli* strains through genome mining tools: an antiSMASH study. *AMB Express* **2022**, *12*, 74.
(7) Reitz, Z. L.; Medema, M. H. Genome mining strategies for metallophore discovery. *Curr. Opin. Biotechnol.* **2022**, *77*, 102757.
(8) Carroll, C. S.; Moore, M. M. Ironing out siderophore biosynthesis: a review of non-ribosomal peptide synthetase (NRPS)-independent siderophore synthetases. *Crit. Rev. Biochem. Mol. Biol.* **2018**, *53*, 356−381.
(9) Challis, G. L. A widely distributed bacterial pathway for siderophore biosynthesis independent of nonribosomal peptide synthetases. *ChemBioChem* **2005**, *6*, 601−611.
(10) Perdicaris, S.; Vlachogianni, T.; Valavanidis, A. Bioactive natural substances from marine sponges: new developments and prospects for future pharmaceuticals. *Nat. Prod. Chem. Res.* **2013**, *01*, 2329−6836.
(11) Anjum, K.; Abbas, S. Q.; Shah, S. A.; Akhter, N.; Batool, S.; Hassan, S. S. Marine sponges as a drug treasure. *Biomol. Ther.* **2016**, *24*, 347−362.
(12) Bibi, F.; Faheem, M.; Azhar, E. I.; Yasir, M.; Alvi, S. A.; Kamal, M. A.; Ullah, I.; Naseer, M. I. Bacteria from marine sponges: a source of new drugs. *Curr. Drug Metab.* **2017**, *18*, 11−15.
(13) Indraningrat, A. A.; Smidt, H.; Sipkema, D. Bioprospecting sponge-associated microbes for antimicrobial compounds. *Mar. Drugs* **2016**, *14*, 87.
(14) Mohite, O. S.; Jørgensen, T. S.; Booth, T. J.; Charusanti, P.; Phaneuf, P. V.; Weber, T.; Palsson, B. O. Pangenome mining of the *Streptomyces* genus redefines species' biosynthetic potential. *Genome Biol.* **2025**, *26*, 9.
(15) Belknap, K. C.; Park, C. J.; Barth, B. M.; Andam, C. P. Genome mining of biosynthetic and chemotherapeutic gene clusters in *Streptomyces* bacteria. *Sci. Rep.* **2020**, *10*, 2003.
(16) Xu, D.; Han, L.; Li, C.; Cao, Q.; Zhu, D.; Barrett, N. H.; Harmody, D.; Chen, J.; Zhu, H.; McCarthy, P. J.; et al. Bioprospecting deep-sea Actinobacteria for novel anti-infective natural products. *Front. Microbiol.* **2018**, *9*, 787.
(17) Blin, K.; Shaw, S.; Vader, L.; Szenei, J.; Reitz, Z. L.; Augustijn, H. E.; Cediel-Becerra, J. D. D.; de Crécy-Lagard, V.; Koetsier, R. A.; Williams, S. E.; et al. antiSMASH 8.0: extended gene cluster detection capabilities and analyses of chemistry, enzymology, and regulation. *Nucleic Acids Res.* **2025**, *53*, W32−W38.
(18) Patzer, S. I.; Braun, V. Gene cluster involved in the biosynthesis of griseobactin, a catechol-peptide siderophore of *Streptomyces* sp. ATCC 700974. *J. Bacteriol.* **2010**, *192*, 426−435.
(19) Yu, W. C.; Yu, Y. L.; Dong, B. C.; Wang, Z. Y.; Du, A. Q.; Li, S. W.; Basnet, B. B.; Bao, X. Z.; Sun, X. R.; Li, X. N.; et al. Targeted discovery of aromatic glycosides with dual detoxification effects via a highly customized molecular networking platform. *Cell Chem. Biol.* **2025**, *33*, 132−144.e9.
(20) Bergstrom, C. P.; Lu, M. C.; Bell, C. L. NMR studies of dimeric 2,3-dihydroxy-N-benzoyl serine. *J. Nat. Prod.* **1991**, *54*, 1003−1008.
(21) Moreno, M.; Zacarias, A.; Porzel, A.; Velasquez, L.; Gonzalez, G.; Alegría-Arcos, M.; Gonzalez-Nilo, F.; Gross, E. K. U. IR and NMR spectroscopic correlation of enterobactin by DFT. *Spectrochim. Acta, Part A* **2018**, *198*, 264−277.
(22) Bachmann, B. O.; Ravel, J. Chapter 8. Methods for *in silico* prediction of microbial polyketide and nonribosomal peptide biosynthetic pathways from DNA sequence data. *Methods Enzymol.* **2009**, *458*, 181−217.
(23) Leduc, D.; Battesti, A.; Bouveret, E. The hotdog thioesterase EntH (YbdB) plays a role *in vivo* in optimal enterobactin biosynthesis by interacting with the ArCP domain of EntB. *J. Bacteriol.* **2007**, *189*, 7112−7126.
(24) Wen, Y.; Wu, X.; Teng, Y.; Qian, C.; Zhan, Z.; Zhao, Y.; Li, O. Identification and analysis of the gene cluster involved in biosynthesis of paenibactin, a catecholate siderophore produced by *Paenibacillus elgii* B69. *Environ. Microbiol.* **2011**, *13*, 2726−2737.
(25) Rauscher, L.; Expert, D.; Matzanke, B. F.; Trautwein, A. X. Chrysobactin-dependent iron acquisition in *Erwinia chrysanthemi*. Functional study of a homolog of the *Escherichia coli* ferric enterobactin esterase. *J. Biol. Chem.* **2002**, *277*, 2385−2395.
(26) Zhu, M.; Valdebenito, M.; Winkelmann, G.; Hantke, K. Functions of the siderophore esterases IroD and IroE in iron-salmochelin utilization. *Microbiol.* **2005**, *151*, 2363−2372.
(27) Müller, S. I.; Valdebenito, M.; Hantke, K. Salmochelin the long-overlooked catecholate siderophore of *Salmonella*. *BioMetals* **2009**, *22*, 691−695.
(28) Baster, Z.; Russell, L.; Rajfur, Z. A review of talin- and integrin-dependent molecular mechanisms in cancer invasion and metastasis. *Int. J. Mol. Sci.* **2025**, *26*, 1798.
(29) Klapholz, B.; Brown, N. H. Talin − the master of integrin adhesions. *J. Cell Sci.* **2017**, *130*, 2435−2446.
(30) Xu, D.; Nepal, K. K.; Chen, J.; Harmody, D.; Zhu, H.; McCarthy, P. J.; Wright, A. E.; Wang, G. Nocardiopsistins A-C: new angucyclines with anti-MRSA activity isolated from a marine sponge-derived *Nocardiopsis* sp. HB-J378. *Synth. Syst. Biotechnol.* **2018**, *3*, 246−251.
(31) Wright, A. E.; Botelho, J. C.; Guzman, E.; Harmody, D.; Linley, P.; McCarthy, P. J.; Pitts, T. P.; Pomponi, S. A.; Reed, J. K. Neopeltolide, a macrolide from a lithistid sponge of the family Neopeltidae. *J. Nat. Prod.* **2007**, *70*, 412−416.
(32) Baster, Z.; Li, L.; Kukkurainen, S.; Chen, J.; Pentikäinen, O.; Győrffy, B.; Hytönen, V. P.; Zhu, H.; Rajfur, Z.; Huang, C. Cyanidin-3-glucoside binds to talin and modulates colon cancer cell adhesions and 3D growth. *FASEB J.* **2020**, *34*, 2227−2237.
(33) Wu, Z.; Li, X.; Sunkara, M.; Spearman, H.; Morris, A. J.; Huang, C. PIPKIγ regulates focal adhesion dynamics and colon cancer cell invasion. *PLoS One* **2011**, *6*, No. e24775.
(34) Li, L.; Kołodziej, T.; Jafari, N.; Chen, J.; Zhu, H.; Rajfur, Z.; Huang, C. Cdk5-mediated phosphorylation regulates phosphatidylinositol 4-phosphate 5-kinase type I γ 90 activity and cell invasion. *FASEB J.* **2019**, *33*, 631−642.
(35) Li, L.; Li, X.; Qi, L.; Rychahou, P.; Jafari, N.; Huang, C. The role of talin2 in breast cancer tumorigenesis and metastasis. *OncoTargets* **2017**, *8*, 106876−106887.
(36) Xu, D.; Tian, E.; Kong, F.; Hong, K. Bioactive molecules from mangrove *Streptomyces qinglanensis* 172205. *Mar. Drugs* **2020**, *18*, 255.
(37) Sun, Y.; He, X.; Liang, J.; Zhou, X.; Deng, Z. Analysis of functions in plasmid pHZ1358 influencing its genetic and structural stability in *Streptomyces lividans* 1326. *Appl. Microbiol. Biotechnol.* **2009**, *82*, 303−310.
(38) Kieser, T.; Bibb, M. J.; Buttner, M. J.; Chater, K. F.; Hopwood, D. A. *Practical Streptomyces Genetics*; John Innes Foundation: Norwich, 2000.

https://doi.org/10.1021/acschembio.6c00106
ACS Chem. Biol. XXXX, XXX, XXX−XXX